JPE 18-1-9

https://doi.org/10.6113/JPE.2018.18.1.92
ISSN(Print): 1598-2092 / ISSN(Online): 2093-4718

Sliding Mode Control for Servo Motors Based on the Differential Evolution Algorithm

Zhonggang Yin†, Lei Gong*, Chao Du*, Jing Liu*, and Yanru Zhong*

†,*Department of Electrical Engineering, Xi'an University of Technology, Xi'an, China

Abstract

A sliding mode control (SMC) for servo motors based on the differential evolution (DE) algorithm, called DE-SMC, is proposed in this study. The parameters of SMC should be designed exactly to improve the robustness, realize the precision positioning, and reduce the steady-state speed error of the servo drive. The main parameters of SMC are optimized using the DE algorithm according to the speed feedback information of the servo motor. The most significant influence factor of the DE algorithm is optimization iteration. A suitable iteration can be achieved by the tested optimization process profile of the main parameters of SMC. Once the parameters of SMC are optimized under a convergent iteration, the system realizes the given performance indices within the shortest time. The experiment indicates that the robustness of the system is improved, and the dynamic and steady performance achieves the given performance indices under a convergent iteration when motor parameters mismatch and load disturbance is added. Moreover, the suitable iteration effectively mitigates the low-speed crawling phenomenon in the system. The correctness and effectiveness of DE-SMC are verified through the experiment.

Key words: Differential evolution (DE) algorithm, Iteration, Parameter optimization, Robustness, Sliding mode control (SMC)

NOMENCLATURE

α, β	Stationary reference frame axes
d, q	Rotary reference frame axes
i_α, i_β	α- and β-Axes stator currents, A
i_d, i_q	d- and q-Axes stator currents, A
i_a, i_b	a- and b-Axes stator currents, A
u_α, u_β	α- and β-Axes stator voltages, V
u_d, u_q	d- and q-Axes stator voltages, V
ψ_d, ψ_q	d- and q-Axes rotor flux linkages, Wb
L_d, L_q	d- and q-Axes stator inductance, H
ψ_f	Flux linkage of permanent magnet, Wb
U_{dc}	DC link voltage, V
□*	Reference quantity
J	Moment of inertia
θ	Rotor position, rad
B	Viscous friction coefficient
ω	Electrical angular velocity, rad/s
R_s	Stator resistance, Ω
T_L	Load torque, N·m
T_e	Electrical magnetic torque, N·m
n_p	Number of pole pairs
P_N	Rated power, kW
U_N	Rated voltage, V
I_N	Rated current, A
f_N	Rated frequency, Hz
n_N	Rated speed, r/min
K_v	Voltage amplification factor
β	Current feedback factor
T_i	Time constant of inertial element
K_{pi}	Proportional factor of the current regulator
K_{pn}	Proportional factor of the speed regulator
τ_n	Integration time constant of the speed regulator
T_m	Electromechanic time constant
K_{fn}	Speed feedback factor
K_ϕ	Electromotive force factor
τ_i	Integration time constant of the current regulator

Manuscript received May 26, 2017; accepted Sep. 6, 2017
Recommended for publication by Associate Editor Gaolin Wang.
†Corresponding Author: zhgyin@xaut.edu.cn
Tel: +86-029-86312650, Xi'an University of Technology
*Dept. of Electrical Engineering, Xi'an University of Technology, China

I. INTRODUCTION

A servo motor can be controlled similarly as a DC motor using the field-oriented control (FOC) approach, and the performance of a servo motor with FOC is comparable with

those of DC motors. As modern industrialization and the permanent magnet material develop, the AC servo drive system with a permanent magnet synchronous motor (PMSM) has been widely used in many areas. However, a series of challenging problems remains in servo motor drives due to parameter variations, model mismatch, unknown disturbances, and the highly nonlinear nature of these drives. These issues contribute to the deterioration of performance of servo drive systems, such as the low-speed crawling phenomenon [1], [2], poor robustness, and inaccurate positioning.

With the rapid development of control theory, several advanced control methods have been proposed to achieve high-precision positioning control performance; these methods include the sliding model control (SMC) [3]-[5], the adaptive control [6]-[8], the internal model control [9]-[12], the active disturbance rejection control (ADRC) [13], [14], and other advanced control technologies. Among these methods, the SMC strategy has many advantages for uncertain systems and parameter mismatch, such as having a simple structure, strong robustness, and extensive applications. Thus, SMC plays a vital role and has practical value in servo drive systems. In particular, SMC is independent of the object model, is insensitive to the variation of system parameters, can restrain disturbance effectively, and can improve system robustness. Therefore, SMC is a practical method for solving the parameter mismatch problem in servo drive systems.

As a robust control method, SMC can deal with the uncertainty of a motor system. Therefore, it is widely applied in many technical fields, particularly in the field of motor control. Many studies have been conducted to improve the robustness of PMSM [15]-[17]. The switched reluctance motor control method based on SMC was applied in [18]. SMC was used for a medium-stroke voice coil motor to achieve position control in [19]. An SMC strategy for electrical line-shafting control for motor speed synchronization was utilized in [20]. A robust control method with high-precision motion control was presented for the positioning control of permanent magnet iron core synchronous motor drives [21]. Most of these works are based on the conventional SMC and are limited to a single control object without model mismatch. Therefore, these existing SMC methods do not illustrate the tuning of SMC parameters in motor control. Few studies involve the positioning control of servo motors based on SMC. Precise positioning is a key index for judging servo drive performance. Several methods for positioning control were proposed in [22], [23]. A flexure-based Lorentz motor fine stage was designed concurrently with a simple proportional–integral–derivative (PID) controller for dual-stage positioning based on the existing coarse stage [22]. However, PID controllers are not robust and their performance deteriorates when the operating conditions change due to parameter variations in the motor. Adaptive backstepping control was applied in [23]. To improve positioning precision, the adaptive law based on neural networks was proposed to tune parameters; however, the robustness of the adaptive backstepping control is worse than that of SMC. When the structure of a controller is considered, SMC is a better choice for applications in servo drive systems. It has a direct and significant impact on system response performance due to the precise positioning requirement of industrial applications. Thus, the SMC structure must be designed accurately; that is, the parameters of SMC must be chosen precisely. Therefore, the tuning of parameters is a significant step in system design. In general, an SMC designer adopts a trial-and-error tuning method. However, the process of manually tuning SMC parameters is time-consuming and requires a considerable amount of design effort. In addition, satisfactory control performance is difficult to achieve in real time. Furthermore, the ranges of certain parameters vary according to different controlled objects. If parameters are not tuned properly, then the performance of SMC will be affected, thereby limiting the extensive application of this method. Therefore, an ideal method for tuning SMC parameters in servo drive systems should be designed.

On the basis of previous works, an SMC based on the differential evolution (DE) algorithm (i.e., DE-SMC) for servo drive systems is proposed in this study. The DE algorithm is adopted to optimize the parameters of SMC. This algorithm is known for its simplicity and rapid performance. The advantages of SMC and the DE algorithm are combined, and the DE algorithm is used to optimize the parameters of SMC with a suitable iteration. DE-SMC improves the robustness of servo drive systems and achieves the given control indices when motor parameters mismatch and load disturbance is added. Meanwhile, the low-speed crawling phenomenon of servo drive systems is mitigated and the given indices are realized after a convergent iteration. The correctness and effectiveness of the proposed method are verified by the experimental results.

II. SMC OF SERVO DRIVE SYSTEMS

A. Mathematical Model of a Servo Drive System

If the servo motor is an ideal controlled object, then the mathematical model of the servo motor under the *d–q* coordinate system is given as follows:

$$\begin{bmatrix} \dot{i}_q \\ \dot{i}_d \\ \dot{\omega} \end{bmatrix} = \begin{bmatrix} -R_s/L_d & -n_P\omega & -n_P\varphi_n/L_d \\ n_P\omega & -R_s/L_d & 0 \\ 1.5n_P\varphi_n/J & 0 & -B/J \end{bmatrix} \cdot \begin{bmatrix} i_q \\ i_d \\ \omega \end{bmatrix} + \begin{bmatrix} u_q/L_d \\ u_d/L_d \\ -T_L/J \end{bmatrix}, \tag{1}$$

$$\begin{bmatrix} \psi_d \\ \psi_q \end{bmatrix} = \begin{bmatrix} L_d & 0 \\ 0 & L_q \end{bmatrix} \cdot \begin{bmatrix} i_d \\ i_q \end{bmatrix} + \begin{bmatrix} \psi_f \\ 0 \end{bmatrix}, \tag{2}$$

$$\begin{bmatrix} u_d \\ u_q \end{bmatrix} = \begin{bmatrix} R_s + dL_d/dt & -\omega L_q \\ \omega L_d & R_s + dL_q/dt \end{bmatrix} \cdot \begin{bmatrix} i_d \\ i_q \end{bmatrix} + \begin{bmatrix} 0 \\ \omega \psi_f \end{bmatrix}, \quad (3)$$

$$T_e = 1.5 n_p [\psi_f i_q + (L_d - L_q) i_q i_d]. \quad (4)$$

On the basis of motor characteristic, $L_d = L_q$, and the servo motor uses the rotor flux oriented vector control technology, which indicates that $i_d = 0$. Then, Eq. (1) becomes

$$\begin{bmatrix} \dot{i}_q \\ \dot{\omega} \end{bmatrix} = \begin{bmatrix} -R_s/L_d & -n_P\varphi_n/L_d \\ 1.5 n_P \varphi_n/J & -B/J \end{bmatrix} \cdot \begin{bmatrix} i_q \\ \omega \end{bmatrix} + \begin{bmatrix} u_q/L_d \\ -T_L/J \end{bmatrix}. \quad (5)$$

The voltage equation is given as

$$\begin{bmatrix} u_d \\ u_q \end{bmatrix} = \begin{bmatrix} R_s + dL_d/dt & -\omega L_q \\ 0 & R_s + dL_q/dt \end{bmatrix} \cdot \begin{bmatrix} 0 \\ i_q \end{bmatrix} + \begin{bmatrix} 0 \\ \omega \psi_f \end{bmatrix}. \quad (6)$$

The torque equation is given as

$$T_e = 1.5 n_p \psi_f i_q. \quad (7)$$

The servo motor motion formula is

$$T_e - T_L = \frac{J}{n_p} \frac{d\omega}{dt}. \quad (8)$$

The conventional servo drive system contains three loops: current, speed, and position loops. From the mathematical model of the motor structure, the design of each loop is shown as follows:

1) Design of the Current Regulator

The control object of the current regulator is described as

$$G_{iobj}(s) = \frac{K_v K_m \beta}{(T_{li}s + 1)(T_i s + 1)}, \quad (9)$$

where $K_m = 1/R_s$ and $T_{li} = L_q/R_s$. The PI controller and the open-loop transfer function of the current loop are described as

$$G_{ACR}(s) = \frac{K_{pi}(\tau_i s + 1)}{\tau_i s}, \quad (10)$$

$$G_{ik}(s) = G_{iobj}(s) \cdot G_{ACR}(s) = \frac{K_v K_m \beta}{(T_{li}s + 1)(T_i s + 1)} \cdot \frac{K_{pi}(\tau_i s + 1)}{\tau_i s}. \quad (11)$$

2) Design of the Speed Regulator

The control object of the current regulator and the PI controller of the speed loop are described as

$$G_{nobj}(s) = \frac{K_l R_s K_{fn}/T_m K_\phi}{s(T_{\Sigma n}s + 1)}, \quad (12)$$

$$G_{ASR}(s) = \frac{K_{pn}(\tau_n s + 1)}{\tau_n s}, \quad (13)$$

where K_{pn} and τ_n are the proportional factor and the integration time constant of the speed regulator, respectively. $T_{\Sigma n}$ is the small inertia time constant. $K_l = 1/\beta$, $K_T = n_p/\psi_f$, and $T_m = J \cdot R_s/(9.55 \cdot K_\phi \cdot K_T)$. The open-loop transfer function of the speed loop is

$$G_{nk}(s) = G_{nobj}(s) \cdot G_{ASR}(s) = \frac{9.55 \cdot K_{fn} K_l K_T K_{pn}(\tau_n s + 1)}{J\tau_n s^2 (T_{\Sigma n}s + 1)}. \quad (14)$$

3) Design of the Position Regulator

The speed loop is a typical II system. It is combined with the position loop to obtain a higher-order system. To conveniently analyze the system, the transfer function of the speed loop and the open-loop transfer function of the position loop are

$$G_{bn}(s) = \frac{K_w}{T_w s + 1}, \quad (15)$$

$$G_{wk}(s) = \frac{K_{pw} K_w}{9.55 s (T_w s + 1)}, \quad (16)$$

where K_w is obtained using the reference and actual speeds, and T_w is the time constant of the inertial element. K_{pw} is the proportional factor of the position regulator.

To improve the robustness of a servo drive system, the conventional speed regulator based on PI is replaced with SMC. The design details of SMC are as follows.

B. Design of SMC

SMC is a nonlinear control method, and the sliding mode can be designed to adapt to the structures of different systems. SMC is independent of the parameters of the controlled object and outside disturbance, and it can be conveniently realized physically. These features have expanded the applications of SMC under different control requirements. However, SMC control is discontinuous and the structure of an SMC system is not fixed. To improve control capability, the structure and relative parameters of SMC should be changed purposefully according to control performance indices. Therefore, the principle and basic design of SMC in a servo drive system is introduced as follows.

Assume that the system is nonlinear and the model is shown in Eq. (17):

$$\dot{x} = f(x,u,t), x \in R^n, u \in R^m, t \in R. \quad (17)$$

In this study, a switching function $s(x)$, which contributes to establishing a variable structure control, should be ensured, and u is shown in Eq. (18):

$$u = \begin{cases} u^+(x), s(x) > 0 \\ u^-(x), s(x) < 0 \end{cases}, \quad (18)$$

where $u^+(x) \neq u^-(x)$. The mathematical formula for the sliding mode existence is described as

$$\begin{cases} \lim\limits_{s \to +0} \dot{s}(x) < 0 \\ \lim\limits_{s \to -0} \dot{s}(x) > 0 \end{cases}. \quad (19)$$

Another way to express the accessibility condition is

$$s(x) \cdot \dot{s}(x) < 0. \quad (20)$$

When the system is in sliding mode, $s(x) = 0$ and $\dot{s}(x) = 0$.

In general, the exponential reaching law section is

$ds/dt=-c\cdot s$, and its solution is shown in Eq. (21):

$$s=s(0)\cdot e^{-ct}. \tag{21}$$

The exponential reaching law section can guarantee that the system approaches sliding mode rapidly given that s is high. However, the single Eq. (21) cannot ensure that the system will arrive at the switching manifold in finite time. To make the reaching rate unequal to zero, the equal rate reaching law section $ds/dt=-\varepsilon\cdot\mathrm{sgn}(s)$ is added. Vibration can be decreased by appropriately changing parameters c and ε, and the reaching rate can be accelerated. Thus, the key points of sliding mode motion are the parameters of the reaching law in Eq. (22) and the switching function.

$$ds/dt=-\varepsilon\cdot\mathrm{sgn}(s)-c\cdot s \tag{22}$$

The reaching law shown in Eq. (22) is selected to design the SMC of the servo drive system. To achieve speed regulation control of the system, the speed error is denoted as $e=\omega^*-\omega$, where ω^* is the reference angular velocity. Thus, the servo motor speed error can be expressed to indicate $x_1=e$ and $x_2=\dot{e}$, and the relative state equation is obtained as

$$\begin{cases} x_1=\omega^*-\omega \\ x_2=\dot{x}_1=\dot{\omega}^*-\dot{\omega} \end{cases}. \tag{23}$$

When Eqs. (8) and (23) are combined, the following expression is obtained:

$$x_2=\dot{x}_1=-\dot{\omega}=-\frac{n_p}{J}(T_e-T_L). \tag{24}$$

The following expression is derived by introducing Eq. (7) into Eq. (24):

$$x_2=-\frac{n_p}{J}(1.5n_p\psi_f i_q-T_L). \tag{25}$$

Again, $\dot{x}_2$ is expressed as

$$\dot{x}_2=-\frac{n_p}{J}(1.5n_p\psi_f\dot{i}_q)=-1.5\frac{n_p^2}{J}\psi_f\dot{i}_q. \tag{26}$$

The mathematical model of the servo drive system at the phase space is

$$\begin{cases} \dot{x}_1=x_2 \\ \dot{x}_2=-A\dot{i}_q \end{cases}, \tag{27}$$

where $A=1.5\frac{n_p^2}{J}\psi_f$. Furthermore, the sliding mode variable s is defined as

$$s=k\cdot x_1+x_2, \tag{28}$$

where k is a positive constant. To quickly reach the sliding surface and reduce chattering, the exponential reaching law is

$$\dot{s}=-\varepsilon\cdot\mathrm{sgn}(s)-c\cdot s, \tag{29}$$

where $\varepsilon>0$ and $c>0$. ε and c are the switching gain and the exponent coefficient of the reaching law, respectively. When the servo drive system is steady, Eq. (30) can be developed as follows:

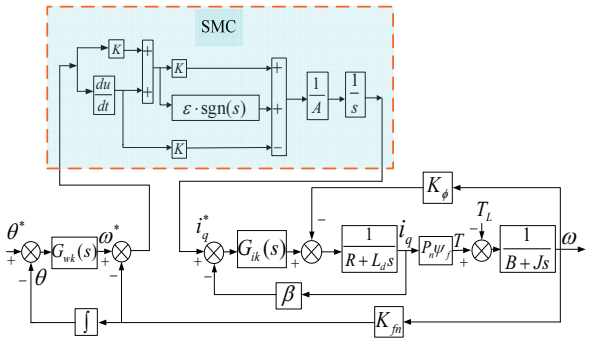

Fig. 1. Diagram of the servo drive system based on SMC.

$$-\varepsilon\cdot\mathrm{sgn}(s)-c\cdot s=k\cdot\dot{x}_1+\dot{x}_2. \tag{30}$$

When Eqs. (25) and (26) are combined, the sliding mode speed controller is

$$\begin{aligned} i_q&=\frac{1}{A}\int(\varepsilon\cdot\mathrm{sgn}(s)+c\cdot s+k\cdot x_2)dt \\ &=\frac{1}{A}\int(k\cdot x_2+\varepsilon\cdot\mathrm{sgn}(s)+c(k\cdot x_1+x_2))dt \\ &=\frac{1}{A}(k+c)\cdot(-\omega)+\frac{1}{A}\int(\varepsilon\cdot\mathrm{sgn}(s)+k\cdot c\cdot(\omega^*-\omega))dt \end{aligned}. \tag{31}$$

The stability analysis of the SMC is verified. In accordance with Lyapunov stability theory, if $\dot{V}(x)=s\cdot\dot{s}\le 0$, then the servo drive system is stable. Thus, Eq. (32) is described by Eqs. (28) and (29).

$$\begin{aligned} \dot{V}(x)&=s\cdot\dot{s}=(k\cdot x_1+x_2)\cdot(-\varepsilon\cdot\mathrm{sgn}(s)-c\cdot s) \\ &=-(k\cdot x_1+x_2)\cdot[\varepsilon\cdot\mathrm{sgn}(k\cdot x_1+x_2)+c\cdot(kx_1+x_2)] \\ &=-\varepsilon\cdot(k\cdot x_1+x_2)\cdot\mathrm{sgn}(k\cdot x_1+x_2)-c\cdot(k\cdot x_1+x_2)^2 \\ &=-\varepsilon\cdot|k\cdot x_1+x_2|-c\cdot(k\cdot x_1+x_2)^2\le 0 \end{aligned} \tag{32}$$

The stability of the SMC is verified according to Eqs. (25) and (26).

Fig. 1 shows the diagram of the servo drive system based on SMC.

III. Optimized SMC Using the DE Algorithm

If the robustness of the servo drive system is improved effectively, then the main SMC parameters, namely, k, ε, and c, must be appropriate. However, suitable parameters for achieving the given performance indices are difficult to select. In this study, the DE algorithm is introduced to optimize the parameters. Thus, the robustness of the system can be strengthened, and its dynamic and steady performance is optimized. The novel DE-SMC method is proposed in this section. It uses the DE algorithm, which can automatically tune the parameters of SMC. Moreover, the experimental results verify that DE-SMC exhibits a better dynamic and steady performance than the ordinary SMC.

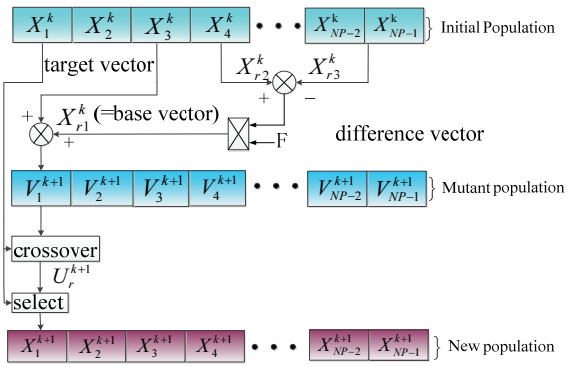

Fig. 2. Main processes of the DE algorithm.

A. Processes of the DE Algorithm

Similar to the principles of other evolutionary algorithms, the DE algorithm is also a multi-point search algorithm. The optimization processes of the DE algorithm are similar to those of the genetic algorithm. The DE algorithm selects two random vectors from the initialization population and then creates a mutant generation through factor F and another random vector. Furthermore, a new generation is evolved and generated via crossover and selection. The main processes of the DE algorithm are illustrated in Fig. 2, and the concrete processes are described as follows.

1) Initialization

Similar to other evolutionary algorithms, the DE algorithm also needs an initial population at the beginning of optimization, and the population size is N_P. The random initial population is from a known range value that covers the entire parameter space.

Set $X_i = [x_{i1}, x_{i2},..., x_{in}]$, where n is the solution space dimension, and an individual vector $X_{i,j}$ is obtained as

$$x_{i,j} = x_{i,j\min} + rand(0,1) * (x_{i,j\max} - x_{i,j\min}), \quad (33)$$

where $x_{i,j}$, $x_{i,jmax}$, and $x_{i,jmin}$ are the j^{th} components, upper limit, and lower limit of individual vector X_i, respectively.

2) Mutation

From the K generation vector X_i^k, the mutated vector $v_{i,j}^{k+1}$ is produced by

$$v_{i,j}^{k+1} = x_{r1,j}^k + \mathrm{F} \cdot (x_{r2,j}^k - x_{r3,j}^k), \quad (34)$$

where $x_{r1,j}^k$, $x_{r2,j}^k$, $x_{r3,j}^k$ are the j^{th} components of three different and random vectors from the K generation individuals. Factor F is a significant parameter for controlling differential quantity.

3) Crossover

The crossover factor is presented to improve the interference vector diversity in the DE algorithm. The target vector $u_{i,j}^{k+1}$ is engendered from mutation and source vectors, and each variable is calculated as

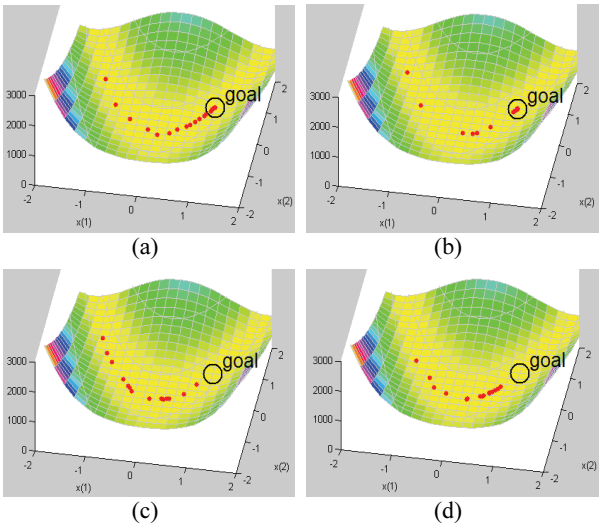

Fig. 3. Main parameters that influence the DE algorithm. (a) F = 0.5, C_R = 0.9, N_P = 100, iterations = 20. (b) F = 0.8, C_R = 0.9, N_P = 100, iterations = 20. (c) F = 0.5, C_R = 0.5, N_P = 100, iterations = 20. (d) F = 0.5, C_R = 0.9, N_P = 100, iterations = 15.

$$u_{i,j}^{k+1} = \begin{cases} v_{i,j}^{k+1} & \eta_j \le \mathrm{C_R} \quad or \quad j = q_j \\ x_{i,j}^k & otherwise \end{cases}, \quad (35)$$

where q_j is a random integer that belongs to (1, n), and $\eta_j \in$ (0, 1) is a random control parameter of the j-dimensional component. The crossover factor $C_R \in (0,1)$ controls the diversity of the population and helps the algorithm escape from the local optimal solution.

4) Selection

In accordance with the principle of greedy selection, if the individual evolution value is better, then the better individual is reserved for a new group. Otherwise, the parent individuals remain in the populations, and this section is described as

$$x_{i,j}^{k+1} = \begin{cases} u_i^{k+1} & if \quad f(u_i^{k+1}) < f(x_i^k) \\ x_i^k & otherwise \end{cases}. \quad (36)$$

The processes of the DE algorithm are described in the preceding paragraphs, and Fig. 3 shows the influences of parameters F and C_R and the number of iterations. In Fig. 3, the red dots represent individuals and the black circle represents the optimization goal. Population quantity N_P is set within the range of 50 to 200. The ranges of F and C_R are (0, 2) and (0, 1), respectively, in the evolution. The mutation factor F determines the ratio of the deviation vector. Figs. 3(a) and 3(b) illustrate that the convergence rate is faster when F is 0.5 than when F is 0.8. When the mutation factor F is small, the convergence rate is fast. The results of the comparison of Figs. 3(a) and 3(c) show that a large crossover factor C_R leads to a fast convergence rate. The results of the comparison of Figs. 3(a) and 3(d) show that more iterations can improve the convergence speed of the DE algorithm. However, more iterations cost considerable time. Thus, the suitable iteration is set from 5 to 50. Finally, the selected parameters of the DE

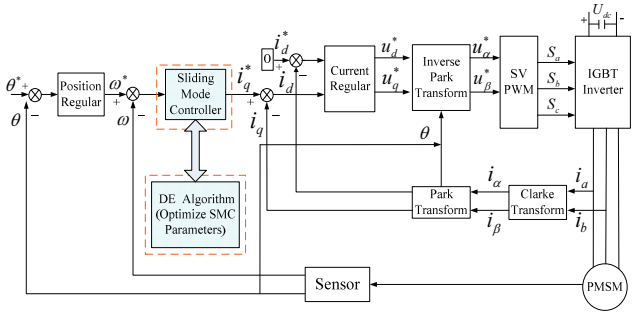

Fig. 4. Structure of the servo drive system based on the DE-SMC method.

algorithm are as follows: $N_P = 100$, $F = 0.5$, and $C_R = 0.9$ in the proposed DE-SMC. The number of iterations depends on the concrete case of the servo drive system.

B. SMC Based on the DE Algorithm for Servo Drive Systems

To study the DE-SMC method for servo drive systems, the structure of DE-SMC based on FOC is shown in Fig. 4. The DE-SMC method mainly comprises two parts to optimize SMC parameters based on the DE algorithm: parameter optimization via the DE algorithm and SMC. From the analysis in Section II, the control performance of SMC is considerably affected by k, ε, and c. Thus, the three variables should be optimized to achieve the given performance indices.

In Fig. 4, i_α and i_β represent the α-axis current and the β-axis stator current, respectively. i_a and i_b represent the a-phase current and the b-phase current, respectively. S_a, S_b, and S_c represent the switching vectors.

The DE algorithm is applied to optimize the three parameters, and thus, improve the control performance of the servo drive system. Then, the concrete processes of applying the DE algorithm to SMC are described as follows.

1) Establishment of the Objective Function

To improve the control performance and robustness of the system, the three key parameters of SMC are optimized using the DE algorithm. Therefore, an objective function, which reflects the performance of the system, is designed to satisfy the control indices.

In general, the performance of a servo drive system includes dynamic performance and steady performance, which mainly include speed rise time T_{rise} and speed steady error E_{ss_spe} (%). If a system is under a rated load and no load, then the given key performance indices are speed drop ΔN_{ovdrop} (%), speed up ΔN_{ovup} (%), recovery time of the rated load T_{rerl}, and recovery time of no load T_{renl}. The corresponding indices of relative performance are described as $T_{rise\text{-}index}$, $E_{ss\_spe\text{-}index}$, $\Delta N_{ovdrop\text{-}index}$, $\Delta N_{ovup\text{-}index}$, $T_{rerl\text{-}index}$, and $T_{renl\text{-}index}$. For the objective function to achieve the control indices in different cases (e.g., parameter mismatch, low-speed crawling, and load disturbance), it should be composed of the weighted sum of the dynamic and given steady performance indices as follows. The objective function is given as

$$Y = k\cdot(T_{rise} - T_{rise-index}) + \varepsilon\cdot(\Delta N_{ovdrop} + \Delta N_{ovup} - \Delta N_{ovdrop-index} - \Delta N_{ovup-index}) + c\cdot(T_{rerl} + T_{renl} + E_{ss\_spe} - T_{rerl-index} - T_{renl-index} - E_{ss\_spe-index}) \tag{37}$$

The objective function of the system is determined by the aforementioned design. That is, when Y is small, the performance of the system is good. Thus, the given performance indices can be achieved until Y reaches the minimum value.

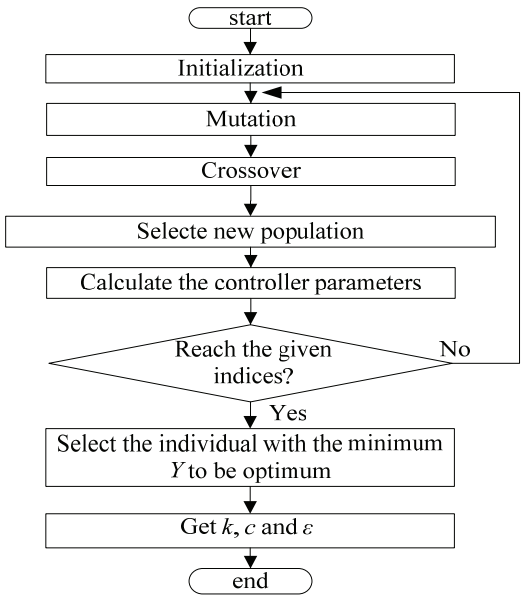

Fig. 5. Main processes of parameter optimization.

2) Parameter Optimization of SMC

The parameters k, ε, and c of SMC are optimized using the DE algorithm according to the objective function and the variables of the system. A series of parameters, namely, T_{rise}, E_{ss_spe}, ΔN_{ovdrop}, ΔN_{ovup}, T_{rerl}, and T_{renl}, are obtained based on the speed feedback; and Y is derived from Eq. (37). First, initial population $Y = [Y_1, Y_2, ..., Y_n]$ and $y_{i,j}$ as the j^{th} component are set. Then, the initial population is mutated by Eq. (20), and the target vector $U_i^{k+1} = [u_{i1}^{k+1}, u_{i2}^{k+1}, ..., u_{in}^{k+1}]$ is calculated from the mutation and source vectors by crossing. The DE algorithm can repeatedly optimize the parameters in the next control cycles and always choose minimum Y from the optimization results. Finally, minimum Y is chosen, which indicates that suitable parameters k, ε, and c are selected and the control performance reaches the given indices. The processes for optimizing k, ε, and c by using the DE algorithm are illustrated in Fig. 5.

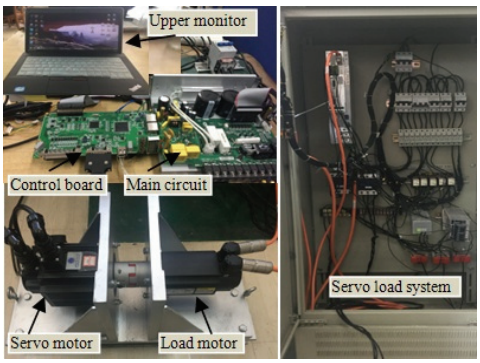

Fig. 6. Experimental platform.

TABLE I
MOTOR PARAMETERS

Symbol	Quantity	Value
P_N	rated power	2 kW
U_N	rated voltage	380V
n_N	rated speed	2500 r/min
I_N	rated torque	7.7N·m
f_N	rated frequence	50Hz
R_s	stator resistance	0.1 Ω
L_d	*d*-Axis stator inductance	24.3mH
L_q	*q*-Axis stator inductance	24.3m H
J	rotational inertia	0.23 kg·m^2
n_p	number of pole pair	4

In the process of optimizing the parameters of SMC using the DE algorithm, the most significant influence factor of servo drive control performance is the number of iterations. Few iterations will result in the failure of the servo drive system to achieve the given performance indices, whereas numerous iterations will increase the required calculation and digital signal processor (DSP) memory resources. Therefore, to achieve the given performance indices after a convergent iteration of the DE algorithm, the relative indices of the control system must be identified first. Then, the optimization process profiles of k, ε, and c are tested, and convergent iteration is achieved.

IV. EXPERIMENTAL RESULTS

The experimental platform is shown in Fig. 6, and the parameters of the servo motor are presented in TABLE I. The platform is built based on the RENESAS DSP SH2A and Lattice field-programmable gate array, and the SMC algorithm is written in C language. The feedback information of the system is delivered to the host computer under the VC ++ environment, the Windows Application Program Interface is used to adopt the USB interface communication method. The DE algorithm is applied to tune the parameters off-line in the host computer.

A. Correctness Verification of DE-SMC

The correctness of DE-SMC under the position control mode is tested with no load, as shown in Figs. 7(a) and 7(b),

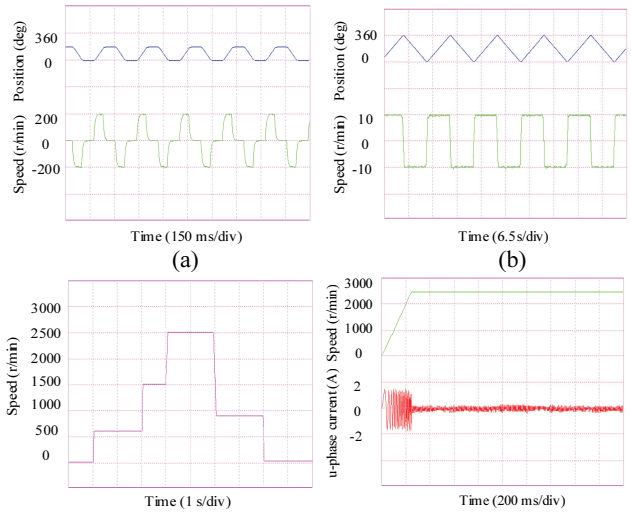

Fig. 7. Responses of position and speed based on DE-SMC. (a) Experimental results when the servo motor switches between 0 and 180 degrees. (b) Experimental results when the servo motor switches between 0 and 360 degrees. (c) Experimental results based on DE-SMC with no load over the speed range. (d) Experimental results when the servo motor starts-up at 2500 r/min based on DE-SMC with no load.

and the input of the system is the reference position (i.e., the number of pulses). The speed of the motor is controlled by the speed of the pulses. Fig. 7(a) shows that the motor switches back and forth between 0 and 180 degrees, and the speed response is ±200 r/min. Fig. 7(b) shows that the motor switches back and forth between 0 and 360 degrees with ±10 r/min. The overshoots of the position and the speed responses are nearly 0, and the motor exhibits good dynamic and steady performance under the position control mode.

The correctness of DE-SMC under the speed control mode is tested with no load, as shown in Figs. 7(c) and 7(d); that is, the input of the system is the reference speed instead of the reference position. Fig. 7(c) shows that the motor runs in six stages: 30, 600, 1500, 2500, 900, and 50 r/min, which represent the full range of running speeds. Fig. 7(d) shows that the motor runs at 2500 r/min in 120 ms, and the overshoot and u-phase currents are approximately 0. That is, DE-SMC demonstrates good start-up dynamic performance under the speed control mode.

The correctness of DE-SMC in the servo drive system is verified effectively under the position control and speed control modes.

B. Effectiveness Verification of DE-SMC

The robustness of the proposed method is mainly investigated under four cases: R_s mismatch, L_d mismatch, low-speed crawling, and load disturbance. If the relative performance of SMC is optimized by the DE algorithm, then the given performance indices should be set first according to the objective function of optimization. The given performance indices are listed in TABLE II.

TABLE II
INDICES OF PARAMETERS

Case	Symbol	Quantity	Index
parameter mismatch	T_{rise}	speed rise time	< 120 ms
parameter mismatch	E_{ss_spe}	speed steady error	< 10%
low speed crawling	E_{ss_spe}	speed steady error	< 10%
low speed crawling	T_{rise}	speed rise time	< 20 ms
load disturbance	ΔN_{ovdrop}	speed drop	< 3%
load disturbance	ΔN_{ovup}	speed up	< 3%
load disturbance	T_{rerl}	recovery time of rated load	< 40 ms
load disturbance	T_{renl}	recovery time of no load	< 40 ms

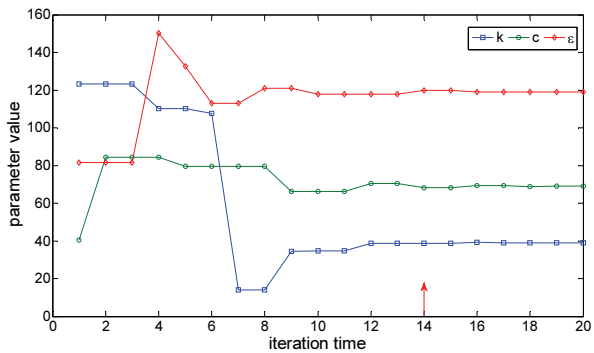

Fig. 8. Optimization processes of the three main parameters.

The optimization processes for the three main parameters k, ε, and c are illustrated in Fig. 8. The servo drive system is steady, and the three parameters are convergent until the 14th iteration, when the system reaches the given performance indices. To verify the correctness of the convergent iteration and the robustness of the system, the system operates under 6th and 14th with different cases. The comparison of the experimental results shows that the system achieves the given performance indices for improving the robustness of a system after a convergent iteration.

1) Verification of Control Performance with R_s Mismatch

Figs. 9 and 10 illustrate the comparative experimental results when the system is under 6th and 14th with R_s mismatch, which aims to improve the dynamic and steady performance of speed response. The position reference switches back and forth between 0 and 360 degrees, and the speed response is ±50 r/min under 6th and 14th with 2 R_s mismatch in Figs. 9(a) and 9(b). Meanwhile, the rise characteristic of speed response is enlarged. The enlarged section shows that the rise time is 32 ms under 6th and 14th. Figs. 9(c) and 9(d) show the steady state errors of speed and position responses when motor speed is +50 r/min. Fig. 10 also verifies the analogous comparative results with 0.5 R_s mismatch. Evidently, the rise time and the steady error of speed and position responses under 14th are smaller than those under 6th. Meanwhile, the speed response reaches the given performance indices until 14th. Therefore, the

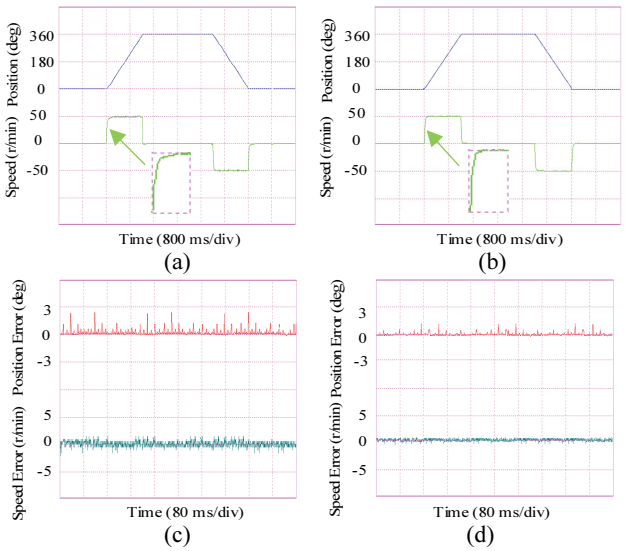

Fig. 9. Comparative results of position and speed responses under 6th and 14th with 2 *Rs*. (a) 6th. (b) 14th. (c) Enlarged figure under 6th. (d) Enlarged figure under 14th.

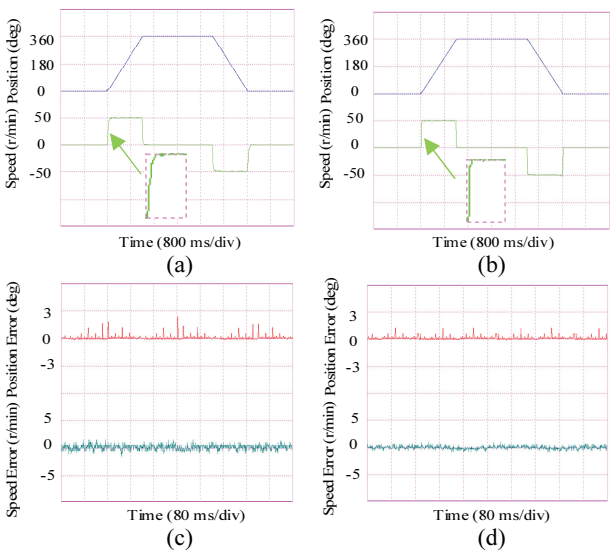

Fig. 10. Comparative results of position and speed responses under 6th and 14th with 0.5 *Rs*. (a) 6th. (b) 14th. (c) Enlarged figure under 6th. (d) Enlarged figure under 14th.

effectiveness of the DE-SMC method with R_s mismatch is verified.

2) Verification of Control Performance with L_d Mismatch

Figs. 11 and 12 illustrate the comparative experimental results when the system is under 6th and 14th with L_d mismatch. When the *d*-axis inductance is under 2 L_d or 0.5 L_d, the position reference switches back and forth between 0 and 360 degrees at ±50 r/min under 6th and 14th in Figs. 11(a) and 11(b), respectively, and the rise characteristic of speed is enlarged. The enlarged section shows that the rise time is 18 ms under 6th and 16 ms under 14th, and the rise time is shorter under 14th. In addition, Figs. 11(c) and 11(d) show the steady state error of speed and position responses when the motor runs at +50 r/min, respectively. Fig. 12 also verifies

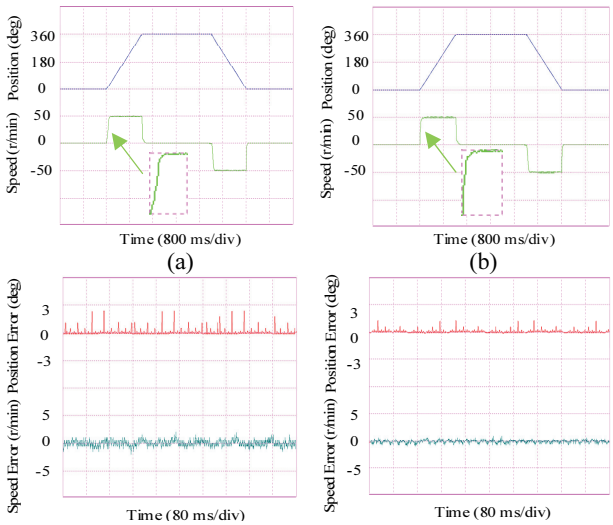

Fig. 11. Comparative results of position and speed responses under 6th and 14th with 2 L_d. (a) 6th. (b) 14th. (c) Enlarged figure under 6th. (d) Enlarged figure under 14th.

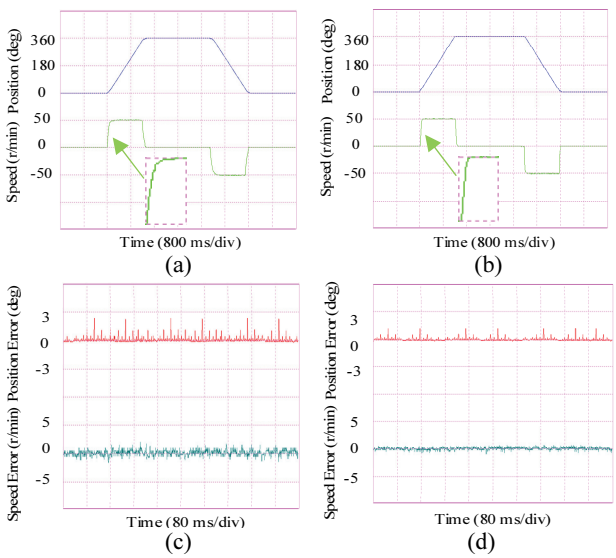

Fig. 12. Comparative results of position and speed responses under 6th and 14th with 0.5 L_d. (a) 6th. (b) 14th. (c) Enlarged figure under 6th. (d) Enlarged figure under 14th.

the analogous comparative results with 0.5 L_d mismatch. Therefore, the steady state errors of speed and position responses evidently decrease, and the speed response is faster under 14th. The relative performance reaches the given performance indices until 14th.

To clearly show the experimental data of control performance under 6th and 14th with parameter mismatch, the histogram of the comparative results is presented in Fig. 13.

3) Verification of Control Performance with Low-speed Crawling

When the system is under the speed control mode, the input of the system is the reference speed. Low-speed crawling is a common phenomenon in servo drive systems.

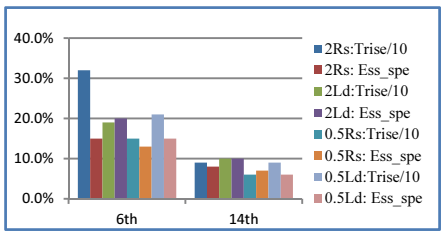

Fig. 13. Comparative histogram of experimental data with parameter mismatch.

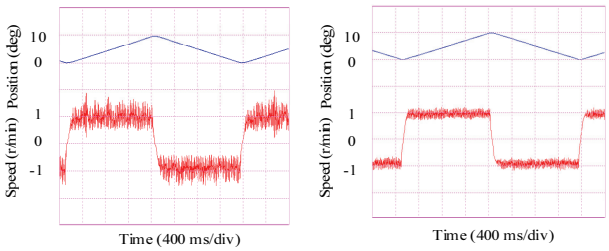

Fig. 14. Comparative results under 6th and 14th with low-speed crawling. (a) 6th. (b) 14th.

The comparative results of the control performance under 6th and 14th are presented. The position reference switches between 0 and 10 degrees at ±1 r/min in Fig. 14. The motor is vibrating at ±1 r/min, and the vibration of the speed response is approximately 0.5 r/min under 6th (E_{ss_spe} = 50%, T_{rise} = 30 ms), as shown in Fig. 14(a), but the speed response is optimized and the vibration is approximately 0.1 r/min under 14th (E_{ss_spe} = 10%, T_{rise} = 20 ms) in Fig. 14(b). The position response is enlarged at +1 r/min under 6th and 14th, as shown in Fig. 15. The comparison of Figs. 15(a) and 15(b) shows that the position response rises more smoothly under 14th, and the vibration of the speed response is evidently decreased. These results effectively validate that the low-speed control performance reaches the control indices under 14th and mitigates the feasibility of the low-speed crawling phenomenon. Therefore, the relative performance of low-speed crawling reaches the given performance indices until 14th.

4) Verification of Control Performance with Load Disturbance

When the system is under the speed control mode, Figs. 16 and 17 show the experimental results of speed response, u-phase current, and torque response under 6th and 14th, respectively. The load steps up from no load to the rated load, and steps down from the rated load to no load. The speed reference is 2500 r/min in Fig. 16 and 250 r/min in Fig. 17. The dynamic performance of step load as it steps up and down is enlarged. Improved robustness and rapid dynamic response are achieved under 14th when the load torque is suddenly varied. Therefore, relative performance reaches the control indices until 14th, and DE-SMC plays an “anti-disturbance” role.

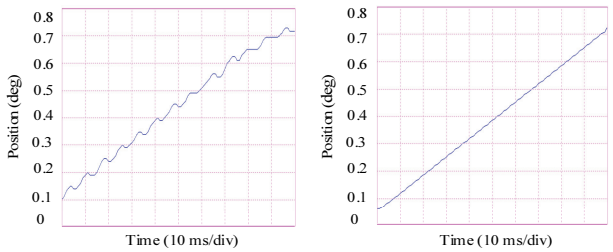

(a) (b)

Fig. 15. Position enlargement under 6th and 14th. (a) 6th. (b) 14th.

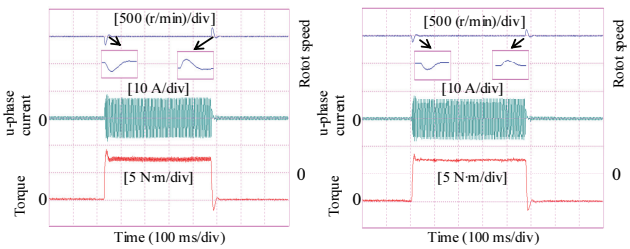

(a) (b)

Fig. 16. Comparative results under 6th and 14th with load disturbance at 2500 r/min. (a) 6th. (b) 14th.

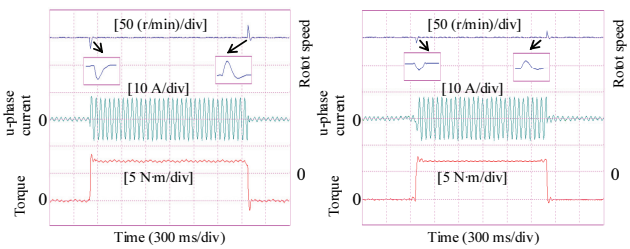

(a) (b)

Fig. 17. Comparative results under 6th and 14th with load disturbance at 250 r/min. (a) 6th. (b) 14th.

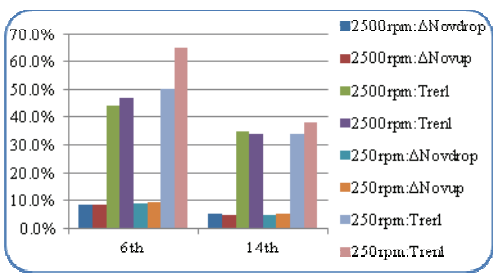

Fig. 18. Histogram of the comparative results under 6th and 14th with load disturbance.

To clearly show the difference in control performance under 6th and 14th with load disturbance, the histogram of the comparative results is presented in Fig. 18.

V. Conclusion

A novel DE-SMC method is applied to a servo drive system. To achieve the given performance indices and improve robustness when the system is under parameter mismatch and load disturbance, a suitable DE algorithm iteration is selected to automatically optimize the main parameters of SMC. The dynamic and given steady performance indices of the speed response in a limited number of iterations can be achieved by the DE algorithm, thereby reducing the low-speed crawling phenomenon under a convergent iteration. That is, robustness can be improved and the given control indices can be achieved under a suitable number of iterations.

Acknowledgment

The authors would like to acknowledge the financial support of the National Natural Science Foundation of China (51677150, 51307139) and the Specialized Research Fund of Shaan Xi Province (2015KJXX-29).

References

[1] Z. Li, J. Chen, G. Zhang, and M. Gan, "Adaptive robust control of servo mechanisms with compensation for nonlinearly parameterized dynamic friction," *IEEE Trans. Control Syst. Technol.*, Vol. 21, No. 1, pp. 194-202, Jan. 2013.

[2] J. Ye, B. Bilgin, and A. Emadi, "An extended-speed low-ripple torque control of switched reluctance motor drives," *IEEE Trans. Power. Electron.*, Vol. 30, No. 3, pp. 1457-1470, Mar. 2015.

[3] J. Y. Hung, W. Gao, and J. C. Hung, "Variable structure control: a survey," *IEEE Trans. Ind. Electron.*, Vol. 40, No. 1, pp. 2-22, Feb. 1993.

[4] H. Castaneda, F. Plestan, A. Chriette, and J. de Leon-Morales, "Continuous differentiator based on adaptive second-order sliding-mode control for a 3-DOF helicopter," *IEEE Trans. Ind. Electron.*, Vol. 63, No. 9, pp. 5786-5793, Sep. 2016.

[5] M. T. Angulo and R. V. Carrillo-Serrano, "Estimating rotor parameters in induction motors using high-order sliding mode algorithms," *IET Control Theory & Applications*, Vol. 9, No. 4, pp. 573-578, Feb. 2015.

[6] A. Saghafinia, H. W. Ping, M. N. Uddin, and K. S. Gaeid, "Adaptive fuzzy sliding-mode control into chattering-free IM drive," *IEEE Trans. Ind. Appl.*, Vol. 51, No. 1, pp. 692-701, Jan./Feb. 2015.

[7] D. Q. Dang, M. S. Rafaq, H. H. Choi, and J.-W. Jung, "Online parameter estimation technique for adaptive control applications of interior PM synchronous motor drives," *IEEE Trans. Ind. Electron.*, Vol. 63, No. 3, pp. 1438-1449, Mar. 2016.

[8] J. W. Jung, V. Q. Leu, T. D. Do, E.-K. Kim, and H. H. Choi, "Adaptive PID speed control design for permanent magnet synchronous motor drives," *IEEE Trans. Power. Electron.*, Vol. 30, No. 2, pp. 900-908, Feb. 2015.

[9] Z. Qiu, M. Santillo, M. Jankovic, and J. Sun, "Composite adaptive internal model control and its application to boost pressure control of a turbocharged gasoline engine," *IEEE Trans. Control Syst. Technol.*, Vol. 23, No. 6, pp. 2306-2315, Nov. 2015.

[10] H. W. Chow and N. C. Cheung, "Disturbance and response time improvement of submicrometer precision linear motion system by using modified disturbance compensator

and internal model reference control," *IEEE Trans. Ind. Electron.*, Vol. 60, No. 1, pp. 139-150, Jan. 2013.
[11] Q. Zhu, Z. G. Yin, Y. Q. Zhang, J. Niu, Y. Li, and Y. Zhong, "Research on two-degree-of-freedom internal model control strategy for induction motor based on immune algorithm," *IEEE Trans. Ind. Electron.*, Vol. 63, No. 3, pp. 1981-1992, Mar. 2016.
[12] X. Sun, Z. Shi, L. Chen, and Z. Yang, "Internal model control for a bearingless permanent magnet synchronous motor based on inverse system method," *IEEE Trans. Energy Convers.*, Vol. 31, No. 4, pp. 1539-1548, Dec. 2016.
[13] L. A. Castaneda, A. Luviano-Juarez, I. Chairez, "Robust trajectory tracking of a delta robot through adaptive active disturbance rejection control," *IEEE Trans. Control Syst. Technol.*, Vol. 23, No. 4, pp. 1387-1398, Jul. 2015.
[14] B. Du, S. P. Wu, S. L. Han, and S. Cui, "Application of linear active disturbance rejection controller for sensorless control of internal permanent-magnet synchronous motorion," *IEEE Trans. Ind. Electron.*, Vol. 63, No. 5, pp. 3019-3027, May 2016.
[15] X. Zhang and G. H. B. Foo, "A robust field-weakening algorithm based on duty ratio regulation for direct torque controlled synchronous reluctance motor," *IEEE/ASME Trans. Mechatronics*, Vol. 21, No. 2, pp. 765-773, Apr. 2016.
[16] X. G. Zhang, L. Sun, K. Zhao, and L. Sun, "Nonlinear speed control for PMSM system using sliding-mode control and disturbance compensation techniques," *IEEE Trans. Power. Electron.*, Vol. 28, No. 3, pp. 1358-1365, Mar. 2013.
[17] S. Li, M. M. Zhou, and X. H. Yu, "Design and implementation of terminal sliding mode control method for PMSM speed regulation system," *IEEE Trans. Ind. Informat.*, Vol. 9, No. 4, pp. 1879-1891, Nov. 2013.
[18] J. Ye, P. Malysz, and A. Emadi, "A Fixed-switching-frequency integral sliding mode current controller for switched reluctance motor drives," *IEEE J. Emerg. Sel. Topics Power Electron*., Vol. 3, No. 2, pp. 381-394, Jun. 2015.
[19] J. F. Pan, S. W. Or, Y. Zou, and N. C. Cheung, "Sliding-mode position control of medium-stroke voice coil motor based on system identification observer," *IET Electric Power Applications*, Vol. 9, No. 9, pp. 620–627, Nov. 2015.
[20] S. Lin, Y. Cai, B. Yang, and W. D. Zhang, "Electrical line-shafting control for motor speed synchronisation using sliding mode controller and disturbance observer," *IET Control Theory & Applications*, Vol. 11, No. 2, pp. 205-212, Jan. 2017.
[21] M. Y. Chen and J. S. Lu, "High-precision motion control for a linear permanent magnet iron core synchronous motor drive in position platform," *IEEE Trans. Ind. Informat.*, Vol. 10, No. 1, pp. 99-108, Feb. 2014.
[22] H. Y. Zhu, C. K. Pang, and T. J. Teo, "Integrated servo-mechanical design of a fine stage for a coarse/fine dual-stage positioning system," *IEEE/ASME Trans. Mechatronics*, Vol. 21, No. 1, pp. 329-338, Feb. 2016.
[23] C. S. Ting, Y. N. Chang, B. W. Shi, and J. F. Lieu, "Adaptive backstepping control for permanent magnet linear synchronous motor servo drive," *IET Electric Power Applications*, Vol. 9, No. 3, pp. 265–279, Mar. 2015.

Zhonggang Yin was born in Shandong, China in 1982. He obtained his B.S., M.S., and Ph.D. in Electrical Engineering from Xi'an University of Technology, Xi'an, China in 2003, 2006, and 2009, respectively. He joined the Electrical Engineering Department of Xi'an University of Technology in 2009, where he is currently a professor. His research interests include high-performance control of AC motors and digital control of power converters.

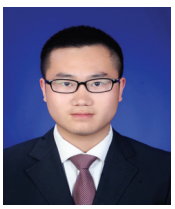

Lei Gong was born in Shaanxi, China in 1993. He obtained his B.S. in Electrical Engineering from Xi'an University of Technology, Xi'an, China in 2015. He is currently working for an M.S. in Electric Machines and Electric Apparatus in Xi'an University of Technology. His main field of interest is the high-performance control of servo motors and the optimization of their efficiency and parameters.

Chao Du was born in Shaanxi, China in 1991. He obtained his B.S. and M.S. in Electrical Engineering from Xi'an University of Technology Xi'an, China in 2013 and 2016, respectively. He is currently working for a Ph.D. in Electrical Engineering in Xi'an University of Technology. His research interests include high- performance AC drive systems and the optimization of their efficiency and parameters.

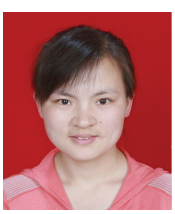

Jing Liu was born in Anhui, China in 1982. She obtained her B.S., M.S., and Ph.D. in Electronic Engineering from Xi'an University of Technology, Xi'an, China in 2003, 2006, and 2009, respectively. She joined the Electronic Engineering Department of Xi'an University of Technology in 2009, where she is currently an associate professor. Her research interests include power semiconductor devices and their application to power electronic devices.

Yanru Zhong was born in Xi'an, China in 1950. He obtained his B.S. in Electrical Engineering from Xi'an Jiaotong University, Xi'an, China in 1975 and his M.S. in Electrical Engineering from Xi'an University of Technology, Xi'an, China in 1983. He joined Xi'an University of Technology in 1983. He was a visiting scholar in the Electrical Engineering Department of Sophia University, Japan in 1987. He has been a professor in Xi'an University of Technology since 1993. He is engaged in research on power electronics, particularly inverter and AC drive systems.